Embedding the dynamics of forced nonlinear systems in multistable memristor circuits

Giacomo Innocenti, Alberto Tesi, Mauro Di Marco, and Mauro Forti

***Abstract*—A well-known feature of memristors is that they makes the circuit dynamics much richer than that generated by classical RLC circuits containing nonlinear resistors. In the case of circuits with ideal memristors, such a multistability property, i.e., the coexistence of many different attractors for a fixed set of parameters, is connected to the fact that the state space is composed of a continuum of invariant manifolds where either convergent or oscillatory and more complex behaviors can be displayed. In this paper we investigate the possibility of designing memristor circuits where known attractors are embedded into the invariant manifolds. We consider a class of forced nonlinear systems containing several systems which are known to display complex dynamics, and we investigate under which conditions the dynamics of any given system of the class can be reproduced by a circuit composed of a two-terminal (one port) element connected to a flux-controlled memristor. It is shown that an input-less circuit is capable to replicate the system attractors generated by varying the constant forcing input, once the parameters of the two-terminal element and the memristor nonlinear characteristic are suitably selected. Indeed, there is a one-one correspondence between the dynamics generated by the nonlinear system for a constant value of the input and that displayed on one of the invariant manifolds of the input-less memristor circuit. Some extensions concerning the case of non-constant forcing terms and the use of charge-controlled memristors are also provided. The results are illustrated via FitzHugh-Nagumo model and Duffing oscillator.**

I. Introduction

Recent years have witnessed a widespread interest in exploring possible ways to alleviate some emerging limitations of digital Von Neumann computing systems [1], [2]. Within this context, in-memory computing is seen as a promising approach to overcome the memory bottleneck related to the strongly increasing amount of data to be processed in solving computational tasks. In-memory computing is based on new nanoscale devices, such as memristors, possessing unconventional features which make it possible to foreseen the development of novel analogue and parallel (neuromorphic) computing schemes [3], [4].

The *ideal* memristor has been introduced in the seminal 1971 paper by Chua [5] as the fourth basic passive circuit element in addition to the resistor, capacitor and inductor. Its constitutive relation is a nonlinear function linking charge to flux (resp., flux to charge) for a flux-controlled (resp., charge-controlled) memristor. In the voltage-current domain an ideal memristor satisfies a state-dependent Ohm's law where the state variable is either the flux, for a flux-controlled memristor, or the charge, for a charge-controlled memristor. Later on, a wider class of memristive systems has been proposed by Chua and Kang in 1976 [6]. These have been further subdivided in *generic* and *extended* memristors, depending upon the complexity of the constitutive relation involving voltage, current and additional memristor internal state variables. We refer the reader to [7] for the nomenclature and a discussion of the hierarchy and genealogy of memristor models used in the literature. Generic and extended memristors are of practical importance in that they can be used to better model some classes of real memristive devices in nanotechnology with respect to ideal memristors [8], [9], [10]. On the other hand, ideal memristors are of great interest in nonlinear circuit theory [11], [12], [13], [14]. Moreover, several articles in the literature discuss physical components or systems whose dynamic behavior can be approximated by that of ideal memristors [15], [16], [17]. In particular, [18], [19] show that in practical ranges of temperature and thickness of the amorphous region, mushroom-type phase-change memory (PCM) and ReRAM devices obey a flux-charge model as that describing ideal memristors. It is also worth to note that numerous analog or digital techniques are available to implement ideal memristors. We refer the reader to [13] and [20] for a detailed account of the current state of the art. Such techniques are based on using current-mode building blocks as second-generation Current Conveyor (CCII), electronically tunable CCII, operational transconductance amplifier (OTA), current feedback operational amplifier (CFOA), differential difference current conveyor, current conveyor transconductance amplifier (CCTA), and differential voltage CCTA. Also, relatively simple structures based on MOS transistors have been proposed (see, e.g., [20] and references therein). Wave-digital emulators of memristors have been devised in [21].

From a dynamic point of view, the key feature of memristors, either ideal or extended and real physical ones, is that their presence makes the circuits capable to generate a large variety of attractors for a fixed set of circuit parameters [12], [22], [23], [24], [25]. This important property is referred to as (extreme) multistability and it is not enjoyed by traditional nonlinear RLC circuits which generally display only a limited number of attractors for any fixed set of circuit parameters. For ideal memristors, it has been shown that multistability is connected to the fact that the state space of memristor circuits is decomposed into a continuum of invariant manifolds [11]. Since on each manifold either convergent or oscillatory and more complex behaviors can be displayed, the coexistence of infinitely many attractors is a natural scenario for circuits with ideal memristors [26], [27], [28], [29], [30], [31], [32]. Moreover, each invariant manifold can be uniquely identified via

G. Innocenti and A. Tesi are with Department of Information Engineering, University of Florence, via S. Marta 3 – 50139 Firenze, Italy

M. Di Marco and M. Forti are with Department of Information Engineering and Mathematics, University of Siena, via Roma 56 – 53100 Siena, Italy.

Corresponding author: G. Innocenti. Email: giacomo.innocenti@unifi.it

some parameters referred to as manifold indexes, whose values depend on the initial conditions of the circuit. By suitably setting these indexes, it is possible to select a desired manifold and also to switch the circuit dynamics between different invariant manifolds and the attractors therein contained [33], [34], [35], [36], [37]. In particular, [37] shows how a shaped voltage/current source can be pulse programmed in order to steer the dynamics from one invariant manifold to another.

The multistability feature of memristors has been thoroughly investigated, also in connection with some classic problems (see, e.g., [38], [39]). However, several interesting issues still deserve to be analyzed. One concerns how many and which type of attractors can be embedded in a memristor circuit, an issue which is certainly appealing from a theoretical point of view since it leads to a better understanding of the richness of the memristor circuits dynamics. It can also have some practical implications, as for instance in the realization of reservoir computing systems [40]. The problem of embedding known dynamics in some system is indeed a classical problem. For instance, a fundamental result of Smale ensures that any dynamic system of order $n-1$ can be embedded in a competitive system of order n (see, e.g., [41] at pp. 344-345). However, this competitive system has not the structure of a circuit or a neural network. Here, we are interested in analyzing how many attractors can be embedded in a system which is implementable via a memristor circuit. Another issue is connected with the role of the input to generate attractors in forced nonlinear systems. For instance, it is well-known that in the FitzHugh-Nagumo model [44], [45] either convergent or oscillatory behaviors are displayed depending on the constant value of the input, i.e., the injected current.

In this paper we investigate how the multistability feature of circuits with an ideal memristor can be exploited to reproduce all the dynamics displayed by a forced nonlinear system. If the forcing input is constant, as in the case of the FitzHugh-Nagumo model, then we consider an input-less memristor circuit whose manifold index is related to the value of the input. If the input is non-constant, as for instance in the case of the Duffing system, then some independent voltage/current sources are introduced in the circuit and programmed according to the index variations. Specifically, the considered class of forced nonlinear systems contains several systems which are known to display complex dynamics, and it is described in Section II together with the memristor circuit to be designed. Such a circuit is assumed to be composed of a finite-dimensional causal linear time-invariant two-terminal (one port) element connected to a flux-controlled ideal memristor. Section III investigates under which conditions an input-less memristor circuit is capable to exactly reproduce the dynamics generated when the nonlinear system is forced by a constant input. Specifically, we look for conditions on the circuit structure which ensure the existence of a one-to-one correspondence between the dynamics of the nonlinear system for a given value of the constant forcing input and that displayed on one of the invariant manifolds. Moreover, a procedure to synthesize the two-terminal element is discussed and its application to the FitzHugh-Nagumo model is illustrated in Section IV. Section V considers the extension to the case when the forcing input of the nonlinear system is no longer constant, by showing that the system dynamics can be still replicated once the two-terminal element is equipped with suitable programmed voltage/current sources. Finally, Section VI considers the case when the flux-controlled memristor is replaced by a charge-controlled one, while some concluding remarks are given in Section VII.

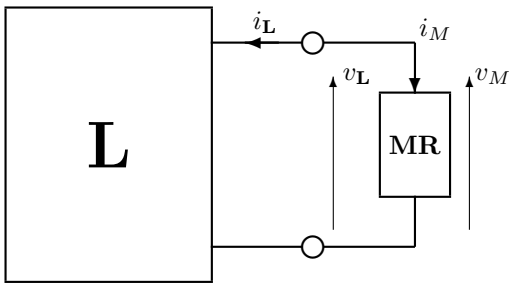

Figure 1. Memristor circuit. $\mathbf{L}$: finite-dimensional causal linear time-invariant two-terminal (one port) element; $\mathbf{MR}$: ideal memristor.

II. Preliminaries and problem formulation

In this paper we consider the class of nonlinear systems which are described by the following state space representation

$$\Sigma: \begin{cases} \dot{x}(t) = Ax(t) + Bf(y(t)) + Du(t) \\ y(t) = Cx(t) \ , \end{cases} \tag{1}$$

where $x \in \mathbb{R}^n$ is the state vector, $u \in \mathbb{R}$ is a scalar input, $y \in \mathbb{R}$ is a scalar output, $A \in \mathbb{R}^{n\times n}$, $B \in \mathbb{R}^{n\times 1}$, $C \in \mathbb{R}^{1\times n}$, $D \in \mathbb{R}^{n\times 1}$. We assume that the nonlinear function $f : \mathbb{R} \to \mathbb{R}$ is such that $f(0) = 0$ and it is sufficiently smooth to ensure existence and uniqueness of the solutions of Σ. The following assumptions are enforced on the matrices A, B, and C.

Assumption 1. The pair (A, B) is controllable and the pair (A, C) is observable.

Also, we initially assume the matrix A is non-singular and the input u is constant over time, i.e.,

$$u(t) = U_0 \qquad \forall t \geq t_0 \ .$$

We observe that the structure of Σ is enjoyed by many systems displaying either convergent or oscillatory and more complex behaviors, such as the FitzHugh-Nagumo model, the Van der Pol and Duffing oscillators, the Chua and Murali–Lakshmanan–Chua circuits.

In the sequel we denote by $x^0(t)$ the solution of (1) for $t \geq t_0$ with initial conditions $x^0(t_0) = x_0$ and constant input U_0. Accordingly, we refer to $\mathcal{S}$ as the set of all the solutions of Σ generated by varying $x_0 \in \mathbb{R}^n$ and $U_0 \in \mathbb{R}$. We find it convenient to write this set as

$$\mathcal{S} = \bigcup_{U_0 \in \mathbb{R}} \mathcal{S}_{U_0} \tag{2}$$

where $\mathcal{S}_{U_0}$ is the set of all the solutions $x^0(t)$ obtained for the fixed input $u(t) = U_0$ by varying the initial conditions $x_0 \in \mathbb{R}^n$.

Our aim is to show that the set $\mathcal{S}$ can be reproduced via the dynamics of the circuit depicted in Fig. 1, which is composed

of a two-terminal (one port) element $\mathbf{L}$, with voltage $v_{\mathbf{L}}$ and current $i_{\mathbf{L}}$, and a memristor $\mathbf{MR}$, with voltage v_M and current i_M.

The two-terminal element $\mathbf{L}$ is either a passive or an active input-less circuit which is described by the following state space representation

$$\mathbf{L}: \begin{cases} \dot{z}(t) = A_L z(t) + B_L i_{\mathbf{L}}(t) \\ v_{\mathbf{L}}(t) = C_L z(t) \ , \end{cases} \tag{3}$$

where $z \in \mathbb{R}^n$, $A_L \in \mathbb{R}^{n\times n}$, $B_L \in \mathbb{R}^{n\times 1}$, $C_L \in \mathbb{R}^{1\times n}$. Clearly, $\mathbf{L}$ admits an input-output description by expressing the Laplace transform of $v_{\mathbf{L}}$ as the product of the Laplace transform of $i_{\mathbf{L}}$ and the equivalent impedance of $\mathbf{L}$ given by

$$L(s) = C_L(sI_n - A_L)^{-1}B_L \ , \tag{4}$$

where I_n is the identity matrix of order n and s is the complex variable.

The memristor $\mathbf{MR}$ is initially assumed to be an ideal flux-controlled memristor and thus described by the nonlinear flux-charge characteristic $N : \mathbb{R} \to \mathbb{R}$, i.e.

$$q_M = N(\varphi_M) \ ,$$

where φ_M and q_M are the memristor flux and charge, whose classic definitions are recalled next [5]:

$$\varphi_M(t) = \int_{-\infty}^{t} v_M(\tau)d\tau \ , \ q_M(t) = \int_{-\infty}^{t} i_M(\tau)d\tau \ .$$

In the voltage-current domain the memristor dynamics is modeled by the following nonlinear system

$$\mathbf{MR}: \begin{cases} \dot{\varphi}_M(t) = v_M(t) \\ i_M(t) = \dot{N}(\varphi_M(t)) = N'(\varphi_M(t))v_M(t) \ , \end{cases} \tag{5}$$

where the derivative $N'(\varphi_M)$ is known as the memconductance of the memristor.

Since $v_{\mathbf{L}} = v_M$ and $i_{\mathbf{L}} = -i_M$ the dynamics of the circuit of Fig. 1 is described by the following equations

$$\Sigma_C: \begin{cases} \dot{z}(t) &= A_L z(t) - B_L \dot{N}(\varphi_M(t)) \\ \dot{\varphi}_M(t) &= C_L z(t) \ . \end{cases} \tag{6}$$

Let $z^0(t)$ and $\varphi_M^0(t)$ be the solution of (6) for $t \geq t_0$ with initial conditions $z^0(t_0) = z_0$ and $\varphi_M^0(t) = \varphi_{M_0}$, and let $\mathcal{S}_C$ denote the set of all the solutions generated by varying $z_0 \in \mathbb{R}^n$ and $\varphi_{M_0} \in \mathbb{R}$. In the next section we determine under which conditions on $\mathbf{L}$ and $\mathbf{MR}$, i.e., on the matrices A_L, B_L, C_L and the memristor nonlinear characteristic $N(\cdot)$, there exists a one-to-one correspondence between $\mathcal{S}_C$ and the solution set $\mathcal{S}$ of Σ.

III. Structure of the dynamically equivalent memristor circuit

It has been shown that the state space of circuits containing an ideal memristors is composed of a continuum of invariant manifolds where either convergent or oscillatory and more complex dynamical behaviors can be displayed (see, e.g., [26] and references therein). These infinitely many invariant manifolds are parameterized by the manifold index $\mathcal{I} \in \mathbb{R}$ whose value determines the specific invariant manifold where the dynamics is confined to lie. A general characterization of the invariant manifolds of the circuit of Fig. 1 Σ_C can be found in [37]. Here, we consider the case when A_L is non-singular.

Proposition III.1. *Let A_L be non-singular. Then, the invariant manifolds of the memristor circuit Σ_C are given by*

$$\mathcal{M}_{\mathcal{I}} = \big\{ z \in \mathbb{R}^n, \varphi_M \in \mathbb{R} : \\ \varphi_M - C_L A_L^{-1} z - C_L A_L^{-1} B_L N(\varphi_M) = \mathcal{I} \big\} \ . \tag{7}$$

Moreover, the following set equivalence

$$\left\{ z \in \mathbb{R}^n, \varphi_M \in \mathbb{R} : \ (z^\top, \ \varphi_M)^\top \in \bigcup_{\mathcal{I}\in\mathbb{R}} \mathcal{M}_{\mathcal{I}} \right\} \equiv \mathbb{R}^{n+1} \tag{8}$$

holds, i.e., the state space of the memristor circuit Σ_C is decomposed into a continuum of invariant manifolds.

Proof. Since A_L is invertible, from the first equation of (6) we get

$$z(t) = A_L^{-1}\left(\dot{z}(t) + B_L \dot{N}(\varphi_M(t))\right)$$

and thus the second equation boils down to

$$\dot{\varphi}_M(t) - C_L A_L^{-1}\dot{z}(t) - C_L A_L^{-1} B_L \dot{N}(\varphi_M(t)) = 0$$

This implies that

$$\sigma(t) \doteq \varphi_M(t) - C_L A_L^{-1} z(t) - C_L A_L^{-1} B_L N(\varphi_M(t))$$

is constant over time, thus showing that $\mathcal{M}_{\mathcal{I}}$ is an invariant manifold. To prove (8) it is enough to observe that for any fixed φ_M all $z \in \mathbb{R}^n$ belong to some manifold $\mathcal{M}_{\mathcal{I}}$. ■

Remark 1. *The above proposition implies that the solution $z^0(t)$, $\varphi_M^0(t)$, $t \geq t_0$, of (6) with initial conditions $z(t_0) = z_0$, $\varphi_M^0(t_0) = \varphi_{M_0}$ is confined to lie onto a specific invariant manifold. Indeed, from the proof it follows the such a solution belongs to the invariant manifold $\mathcal{M}_{\mathcal{I}}$ with*

$$\mathcal{I} = \varphi_{M_0} - C_L A_L^{-1} z_0 - C_L A_L^{-1} B_L N(\varphi_{M_0}) \ . \tag{9}$$

Hence, the initial conditions z_0, φ_{M_0} dictate the invariant manifold $\mathcal{M}_{\mathcal{I}}$ where the solutions are confined to lie.

Proposition III.1 states that the solution set $\mathcal{S}_C$ of (6) can be obtained by collecting the sets of solutions belonging to $\mathcal{M}_{\mathcal{I}}$ for $\mathcal{I} \in \mathbb{R}$, i.e.,

$$\mathcal{S}_C = \bigcup_{\mathcal{I}\in\mathbb{R}} \mathcal{S}_{C_{\mathcal{I}}} \ ,$$

where $\mathcal{S}_{C_{\mathcal{I}}}$ is the set of all the solutions $z^0(t)$, $\varphi_M^0(t)$, $t \geq t_0$, of (6) with initial conditions $z(t_0) = z_0$, $\varphi_M^0(t_0) = \varphi_{M_0}$ such that condition (9) holds.

We are now ready to determine the sought conditions ensuring that there is a one-to-one correspondence between $\mathcal{S}_C$ and the solution set $\mathcal{S}$ in (2). The next result holds true.

Proposition III.2. *Let A be non-singular and suppose that the nonlinear characteristic of $\mathbf{MR}$ is chosen as*

$$N(\cdot) = -f(\cdot) \ . \tag{10}$$

and the matrices of $\mathbf{L}$ are such that

$$A_L = T^{-1}AT \ , \quad B_L = T^{-1}B \ , \qquad C_L = CT \ , \tag{11}$$

where $T \in \mathbb{R}^{n\times n}$ is a non-singular matrix. Then, for any $x_0 \in \mathbb{R}^n$ and $U_0 \in \mathbb{R}$ the solution $x^0(t)$ of (1) for $t \geq t_0$ with initial conditions $x^0(t_0) = x_0$ and input $u(t) = U_0$ can be written as

$$x^0(t) = x_0 + \int_{t_0}^{t} Tz^0(\tau)d\tau \ , \tag{12}$$

where $z^0(t)$ is the solution for $t \geq t_0$ of (6) with initial conditions

$$z_0 = T^{-1}\left(Ax_0 + Bf(Cx_0) + DU_0\right) \ , \quad \varphi_{M_0} = Cx_0 \ . \tag{13}$$

Moreover, $z^0(t)$ belongs to the invariant manifold $\mathcal{M}_{\mathcal{I}}$ with the index given by

$$\mathcal{I} = -CA^{-1}DU_0 \ . \tag{14}$$

Proof. Consider the following equations

$$\begin{cases} \dot{\xi}(t) = A\xi(t) + B\dot{f}(\eta(t)) \\ \dot{\eta}(t) = C\xi(t) \ , \end{cases} \tag{15}$$

which are obtained by first making the time-derivative of equations (1) and then replacing $\dot{x}$ and y with ξ and η, respectively. It can be readily verified that if $x^0(t)$, $t \geq t_0$, is the solution of (1) with initial conditions $x^0(t_0) = x_0$ and input $u(t) = U_0$, then the solution of (15) for $t \geq t_0$ with initial conditions $\xi(t_0) = Ax_0 + Bf(Cx_0) + DU_0$ and $\eta(t_0) = Cx_0$ is given by

$$\begin{cases} \xi(t) = \dot{x}^0(t) \\ \eta(t) = Cx^0(t) \ . \end{cases}$$

Now, the memristor circuit equations (6) with the nonlinear characteristic $N(\cdot)$ and the matrices A_L, B_L, C_L are set according to (10) and (11), respectively, become

$$\begin{cases} \dot{z}(t) = T^{-1}ATz(t) - T^{-1}B\dot{f}(\varphi_M(t)) \\ \dot{\varphi_M}(t) = CTz(t) \ . \end{cases} \tag{16}$$

By comparing (15) and (16) and rewriting the first equation of (16) as $T\dot{z}(t) = ATz(t) - B\dot{f}(\phi(t))$, it readily follows that the solutions $z^0(t)$ and $\varphi_M^0(t)$ of (16) with the initial conditions in (13) are such that

$$\begin{cases} Tz^0(t) = \dot{x}^0(t) \\ \varphi_M^0(t) = Cx^0(t) \ , \end{cases}$$

thus proving relation (12). The assumption that A is non-singular ensures that also A_L is non-singular and thus from Proposition III.1 we have that $z^0(t)$ belongs to an invariant manifold having the structure in (7). Taking into account (10) and (11), (7) can be rewritten as

$$\mathcal{M}_{\mathcal{I}} = \left\{z \in \mathbb{R}^n, \varphi_M \in \mathbb{R} : \varphi_M - CA^{-1}Tz + CA^{-1}Bf(\varphi_M) = \mathcal{I}\right\} \ ,$$

and hence, according to Remark 1, $z^0(t)$ belongs to the invariant manifold $\mathcal{M}_{\mathcal{I}}$ with

$$\mathcal{I} = \varphi_{M_0} - CA^{-1}Tz_0 + CA^{-1}Bf(\varphi_{M_0}) \ .$$

By replacing z_0 with the expression in (13) and taking into account that $\varphi_{M_0} = Cx_0$, we finally get

$$\begin{aligned}\mathcal{I} = \varphi_{M_0} - CA^{-1}\left(Ax_0 + Bf(Cx_0) + DU_0\right) \\ + CA{-}1Bf(\varphi_{M_0}) = -CA^{-1}DU_0 \ .\end{aligned}$$

■

Proposition III.2 provides the conditions under which each solution $x^0(t)$ of Σ is exactly reproduced via a suitable solution $z^0(t)$ of Σ_C, according to (12). We remark that, according to (10), the ideal memristor flux-charge characteristic needs to coincide with the function $f(\varphi)$, which is odd and non-monotone, as in the case of the FitzHugh-Nagumo model of Section IV. Since $N(\cdot)$ is non-monotone, the memristor is active and it can be implemented in a standard way via a passive memristor in parallel to a negative resistor obtained using a current inverter (INIC). We also remark that an odd characteristic of the passive memristor may be obtained for instance by adequately biasing with some adapting circuitry PCM devices [18]. Another possibility is to resort to analog implementations via OTA or CMOS [13], [20] in combination with techniques to symmetrize the flux-charge characteristic as for instance using two memristors in a complementary resistive switching (CRS) configuration. The result in Proposition III.2 can be strengthened as follows.

Proposition III.3. *Let A be non-singular and let conditions (10)-(11) hold. If*

$$CA^{-1}D \neq 0 \ , \tag{17}$$

then there is a one-to-one correspondence between the solution sets $\mathcal{S}$ and $\mathcal{S}_C$ of Σ and Σ_C, respectively.

Proof. If (17) is satisfied then (14) shows that there is a proportional relation between the index $\mathcal{I}$ of the invariant manifold and the value U_0 of the constant input. Hence, it is enough to prove that there exists a one-to-one correspondence between the solution sets $\mathcal{S}_{U_0}$ and $\mathcal{S}_{C_{\mathcal{I}}}$, with U_0 and $\mathcal{I}$ being related via (14).

Recall that $\mathcal{S}_{U_0}$ is the set of all solutions of Σ obtained for a fixed U_0 by varying the initial condition $x_0 \in \mathbf{R}^n$, while $\mathcal{S}_{C_{\mathcal{I}}}$ is the set of all solutions of Σ_C with initial conditions z_0, φ_{M_0} belonging to the following set

$$\mathcal{L}_{\mathcal{I}} = \left\{z_0 \in \mathbb{R}^n, \varphi_{M_0} \in \mathbb{R} : \varphi_{M_0} - CA^{-1}Tz_0 + C_LA^{-1}Bf(\varphi_{M_0}) = \mathcal{I}\right\} \ ,$$

Since $\mathcal{L}_{\mathcal{I}} \equiv \mathbb{R}^n$, to prove one-to-one correspondence between $\mathcal{S}$ and $\mathcal{S}_C$ it is enough to show that there not exist two different solutions in $\mathcal{S}$ to which correspond the same solution in $\mathcal{S}_C$. Hence, let $\bar{x}^0(t)$ and $\hat{x}^0(t)$ denote the solutions in $\mathcal{S}$ with initial conditions $\bar{x}^0(t_0) = \bar{x}_0$ and $\hat{x}^0(t_0) = \hat{x}_0$, $\bar{x}_0 \neq \hat{x}_0$, respectively. From Proposition III.2 we have that the solutions $\bar{z}^0(t)$, $\bar{\varphi}_M^0(t)$ and $\hat{z}^0(t)$, $\hat{\varphi}_M^0(t)$ have the initial conditions $\bar{z}_0$, $\bar{\varphi}_{M_0}$ and $\hat{z}_0$, $\hat{\varphi}_{M_0}$, respectively. According to (13), we have

$$\bar{z}_0 = T^{-1}\left(A\bar{x}_0 + Bf(C\bar{x}_0) + DU_0\right) \ , \ \bar{\varphi}_{M_0} = C\bar{x}_0$$

and

$$\hat{z}_0 = T^{-1}\left(A\hat{x}_0 + Bf(C\hat{x}_0) + DU_0\right) \ , \ \hat{\varphi}_{M_0} = C\hat{x}_0 \ .$$

Clearly, $\bar{z}^0(t)$, $\bar{\varphi}_M^0(t)$ coincides with $\hat{z}^0(t)$, $\hat{\varphi}_M^0(t)$ if and only if $\bar{z}_0 = \hat{z}_0$ and $\bar{\varphi}_{M_0} = \hat{\varphi}_{M_0}$. These two conditions can be equivalently written as

$$A\bar{x}_0 + Bf(C\bar{x}_0) = A\hat{x}_0 + Bf(C\hat{x}_0) \ , \tag{18}$$

and

$$C\bar{x}_0 = C\hat{x}_0 \ , \tag{19}$$

respectively. Exploiting (19), condition (18) boils down to

$$A(\bar{x}_0 - \hat{x}_0) = 0$$

and thus it is solved only if $\bar{x}_0 = \hat{x}_0$, which is a contradiction. ■

Remark 2. *The proof of Proposition III.3 shows that each invariant manifold $\mathcal{M}_{\mathcal{I}}$ replicates all the solutions of* (1) *obtained for a fixed constant input $u(t) = U_0$ once $\mathcal{I}$ and U_0 satisfy the linear relation* (14)*. In the case that Σ displays different attractors for different values of U_0, this relation permits to keep track of the invariant manifolds where these attractors are reproduced. In [37] it has been shown that the introduction of pulse programmed sources in the memristor circuit makes it possible to switch the circuit dynamics between different attractors. This suggests that the case of non-constant input u can be tackled by incorporating suitably designed voltage/current sources in the two-terminal element $\mathbf{L}$ of the circuit of Fig. 1. This issue will be investigated in Section V.*

Proposition III.2 defines the structure that equations (3) and (5) should enjoy to reproduce the solutions of system Σ. Specifically, the flux-controlled memristor is completely designed once the nonlinear characteristic satisfies (10), while different matrices A_L, B_L, and C_L can be chosen by varying the matrix T.

This degree of freedom is used to select a specific circuital realization of the equations (3) governing the two-terminal element. We first observe that for any choice of A_L, B_L, and C_L the impedance (4) of $\mathbf{L}$ satisfies

$$L(s) = C(sI_n - A)^{-1}B \ . \tag{20}$$

Hence, we have to synthesize either a passive or an active two-terminal element $\mathbf{L}$ having such an impedance. This can be done by exploiting one of the available procedures (see, e.g., [42], [43]), together with the impedance scaling technique. Note that Assumption 1 ensures that the strictly proper rational function $L(s)$ has order equal to n. This implies that $\mathbf{L}$ can be synthesized with $n_C \geq 0$ capacitors and $n_L \geq 0$ inductors with $n = n_C + n_L$. Let v_{C_i}, $i = 1, \ldots, n_C$, and i_{L_j}, $j = 1, \ldots, n_L$, denote the voltages of the capacitors and the currents of the inductors, respectively, and consider the state vector $\bar{z} = (v_{C_1}, \ldots, v_{C_{n_C}}, i_{L_1}, \ldots, i_{L_{n_L}}) \in \mathbb{R}^n$. Then, by applying the Kirchhoff's law to the loops and nodes of the synthesized $\mathbf{L}$, we can write the following state space representation

$$\begin{cases} \dot{\bar{z}}(t) = \bar{A}_L\bar{z}(t) + \bar{B}_L i_{\mathbf{L}}(t) \\ v_{\mathbf{L}}(t) = \bar{C}_L\bar{z}(t) \ , \end{cases} \tag{21}$$

for some suitable matrices $\bar{A}_L$, $\bar{B}_L$, and $\bar{C}_L$. Since by construction

$$\bar{C}_L(sI_n - \bar{A}_L)^{-1}\bar{B}_L = L(s) \ , \tag{22}$$

there exists a non-singular matrix $\bar{T} \in \mathbb{R}^{n\times n}$ satisfying (11) , i.e., solving the linear equations

$$A\bar{T} = \bar{T}\bar{A}_L \ , \quad B = \bar{T}\bar{B}_L \ , \quad C\bar{T} = \bar{C}_L \ . \tag{23}$$

Clearly, the designed circuit obeys equations (6) with $A_L = \bar{A}_L$, $B_L = \bar{B}_L$, $C_L = \bar{C}_L$, and $N(\cdot) = -f(\cdot)$ and hence, according to Proposition III.2, it is capable to reproduce all the solutions of Σ. Specifically, the solution $x^0(t)$ of (1) for $t \geq t_0$ with initial conditions $x^0(t_0) = x_0$ and input $u(t) = U_0$ is given by (12) once T is replaced by $\bar{T}$ and $z^0(t)$ is the solution generated by the designed circuit for $t \geq t_0$ with initial conditions as in (13) with T^{-1} replaced by $\bar{T}^{-1}$.

A. The case of singular matrix A

In this subsection we show how the assumption of A being non-singular can be relaxed. Indeed, if the matrix A of Σ is non-invertible we can rewrite equations (1) as

$$\begin{cases} \dot{x}(t) = (A - kBC)x(t) + B(f(y(t)) + ky(t)) + Du(t) \\ y(t) = Cx(t) \ , \end{cases} \tag{24}$$

where $k \in \mathbb{R}$ is a parameter to be chosen such that $\det(A - kBC) \neq 0$. Clearly, for such a k all the results obtained in the case of a non-singular A are still valid once A and $f(y)$ are replaced by $A_k \doteq A - kBC$ and $f_k(y) \doteq f(y) + ky$. In particular, it can be checked that the impedance of the two-terminal element $\mathbf{L}$ to be synthesized becomes

$$L_k(s) = C(sI_n - A_k)^{-1}B = \frac{L(s)}{1 + kL(s)} \ , \tag{25}$$

where $L(s)$ is as in (20). This relation between $L_k(s)$ and $L(s)$ is exploited to show that it is possible to find k such that A_k is non-singular. The next result holds true.

Proposition III.4. *Let Assumption 1 hold and let A be singular. Then, there always exists $k \in \mathbb{R}$ such that*

$$\det(A - kBC) \neq 0 \ .$$

Proof. Observe that $L(s)$ can be expressed

$$L(s) = \frac{C\mathrm{Adj}(sI_n - A)B}{\det(sI_n - A)}$$

and $L_k(s)$ can be written as

$$\begin{aligned} L_k(s) &= \frac{C\mathrm{Adj}(sI_n - A_k)B}{\det(sI_n - A_k)} \\ &= \frac{C\mathrm{Adj}(sI_n - A)B}{\det(sI_n - A) + kC\mathrm{Adj}(sI_n - A)B} \ . \end{aligned}$$

where the second equality follows from (25). Hence, we have the following equality

$$\det(sI_n - A_k) = \det(sI_n - A) + kC\mathrm{Adj}(sI_n - A)B \, .$$

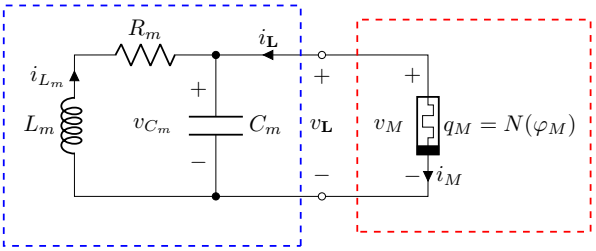

Figure 2. Memristor circuit capable to reproduce the dynamics of the FitzHugh-Nagumo neuron model: the passive two-terminal elementi $\mathbf{L}$ (blue box) with R_m, L_m, and C_m as in (32), and the flux-controlled memristor (red box) with the nonlinear characteristic (30).

which implies that $\det A_k = 0$ if and only if

$$\det(-A) + kC\text{Adj}(-A)B = kC\text{Adj}(-A)B = 0 \ . \qquad (26)$$

Since A is singular, zero is a pole of $L(s)$, and, because Assumption 1 ensures that $L(s)$ cannot have any zero-pole cancellation, $L(s)$ cannot have a zero at $s = 0$ and hence we have that C Adj$(-A)B \neq 0$. This implies that (26) holds only for $k = 0$ and hence we have shown that $\det(A - kBC) \neq 0$ for all $k \neq 0$. ■

Remark 3. *From the proof of Proposition it follows that A_k is non-singular for all $k \neq 0$. This degree of freedom in the choice of k can be used to optimize the synthesis of the impedance of $\mathbf{L}$ and/or the memristor nonlinear characteristic $N(\cdot) = -f_k(\cdot)$. Since Σ can be written in the form (24) even if A is non-singular, it follows that also in this case the parameter k can be chosen to optimize the synthesis of the memristor circuit.*

IV. Application to the FitzHugh-Nagumo model

In this section the application of the previous results will be illustrated by designing a memristor circuit capable to reproduce the dynamics of the FitzHugh-Nagumo neuron model [44], [45], [46], [47], which is a second order approximation of the celebrated Hodgkin-Huxley model [48]. Some other memristive FitzHugh–Nagumo circuits have been already proposed for different purposes [49], [50], [51]. The model FitzHugh-Nagumo equations read

$$\begin{cases} \dot V = V - W - \dfrac{V^3}{3} + I \\ \dot W = a\,(bV - cW) \end{cases} \qquad (27)$$

where V represents the membrane potential, W is an internal variable, the coefficients a, b, c are positive tuning parameters, and I is a constant forcing current, used to stimulate the neuron response. It can be readily verified that model (27) admits the state space representation Σ in (1) once

$$x = \begin{pmatrix} V \\ W \end{pmatrix} \ , \ y = V \ , \ u = I \ , \ f(y) = y - \frac{y^3}{3} \ , \qquad (28)$$

$$A = \begin{pmatrix} 0 & -1 \\ ab & -ac \end{pmatrix} \ , \ B = \begin{pmatrix} 1 \\ 0 \end{pmatrix} \ , \quad D = \begin{pmatrix} 1 \\ 0 \end{pmatrix} \ , \ C = \begin{pmatrix} 1 & 0 \end{pmatrix} \ . \qquad (29)$$

Since $a, b, c > 0$, we have

$$\det A = ab \neq 0 \ , \quad CA^{-1}D = \frac{c}{b} \neq 0 \ ,$$

and hence A is non-singular and condition (17) holds.
To design the memristor circuit of Fig. 1, we first observe that the flux-controlled memristor $\mathbf{MR}$ should be implemented according to equation (5) where the nonlinear characteristic must satisfy (10), which implies

$$N(\varphi_M) = -\varphi_M + \frac{\varphi_M^3}{3} \ . \qquad (30)$$

Exploiting the expression of A, B, and C in (29), we get that the impedance (4) of the two-terminal element $\mathbf{L}$ is given by

$$L(s) = \frac{s + ac}{s^2 + acs + ab} \qquad (31)$$

and, therefore, the corresponding admittance is

$$L^{-1}(s) = \frac{s^2 + acs + ab}{s + ac} = s + \frac{ab}{s + ac} \ .$$

It can readily verified that this admittance can be synthesized via the parallel interconnection of a capacitor C_m with the series of an inductor L_m and a resistor R_m, once

$$R_m = \frac{c}{b} \ , \qquad L_m = \frac{1}{ab} \ , \qquad C_m = 1 \ . \qquad (32)$$

Figure 2 depicts the synthesized circuit whose governing equations are

$$\begin{cases} \dot v_{C_m} = \dfrac{1}{C_m}\,(i_{L_m} - i_M) \\ \dot i_{L_m} = -\dfrac{1}{L_m}\,(v_{C_m} + R_m i_{L_m}) \\ \dot\varphi_M = v_M \end{cases} \qquad (33)$$

where $v_M = v_{C_m}$ and $i_M = \dot N(\varphi_M) = (-1 + \varphi_M^2)v_{C_m}$. Since $i_{\mathbf{L}} = -i_M$ and $v_{\mathbf{L}} = v_{C_m} = v_M$, we get that equations (33) admit the state space representation Σ_C in (6) with $z = (v_{C_m}, i_{L_m})^\top$ and $A_L = \bar A_L$, $B_L = \bar B_L$, and $C_L = \bar C_L$ where

$$\bar A_L = \begin{pmatrix} 0 & \dfrac{1}{C_m} \\ -\dfrac{1}{L_m} & -\dfrac{R_m}{L_m} \end{pmatrix} \ , \quad \bar B_L = \begin{pmatrix} \dfrac{1}{C_m} \\ 0 \end{pmatrix} \ ,$$
$$\bar C_L = \begin{pmatrix} 1 & 0 \end{pmatrix} \ .$$

To apply Propositions III.2 and III.3 it remains to compute the matrix $\bar T$ solving conditions (23). Indeed, we get

$$A\bar T = \begin{pmatrix} -T_{21} & -T_{22} \\ abT_{11} - acT_{21} & abT_{12} - acT_{22} \end{pmatrix}$$
$$= \begin{pmatrix} -\dfrac{1}{L_m}T_{12} & \dfrac{1}{C_m}T_{11} - \dfrac{R_m}{L_m}T_{12} \\ -\dfrac{1}{L_m}T_{22} & \dfrac{1}{C_m}T_{21} - \dfrac{R_m}{L_m}T_{22} \end{pmatrix} = \bar T \bar A_L$$
$$B = \begin{pmatrix} 1 \\ 0 \end{pmatrix} = \begin{pmatrix} \dfrac{1}{C_m}T_{11} \\ \dfrac{1}{C_m}T_{21} \end{pmatrix} = \bar T \bar B_L$$
$$C\bar T = \begin{pmatrix} T_{11} & T_{12} \end{pmatrix} = \begin{pmatrix} 1 & 0 \end{pmatrix} = \bar C_L$$

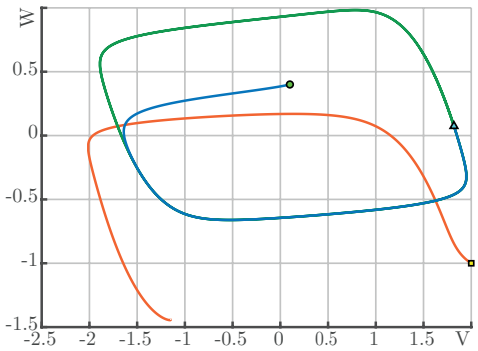

Figure 3. State space orbits of the FitzHugh-Nagumo model (27) for parametric configuration (36). The circle, triangle and square respectively depict the starting points $x_0^{(1)}$, $x_0^{(2)}$, $x_0^{(3)}$ illustrated in Subsection IV-A.

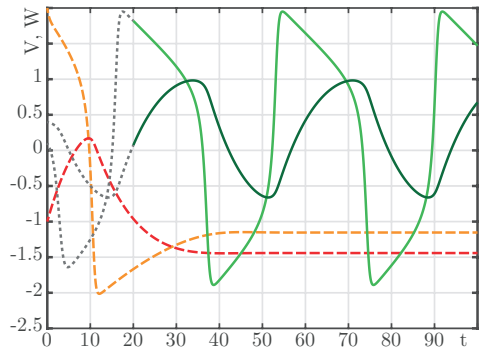

Figure 4. Time representation of the solutions of the FitzHugh-Nagumo model (27) illustrated in Subsection IV-A. The solid curves (initially dotted) depict the behavior of the state variables for the solution starting from the initial condition $x_0^{(1)}$ and passing by $x_0^{(2)}$ at $t = 20$, when the line style changes. The dashed curves regard the solution starting from the initial condition $x_0^{(3)}$.

where T_{ij}, $i = 1, 2$, $j = 1, 2$, are the entries of $\bar{T}$. The above equations boil down to

$$\begin{cases} T_{21} - \dfrac{1}{L_m} T_{12} = 0 \\ T_{22} + \dfrac{1}{C_m} T_{11} - \dfrac{R_m}{L_m} T_{12} = 0 \\ abT_{11} - acT_{21} + \dfrac{1}{L_m} T_{22} = 0 \\ abT_{12} - acT_{22} - \dfrac{1}{C_m} T_{21} + \dfrac{R_m}{L_m} T_{22} = 0 \\ T_{11} = C_m \\ T_{11} = 1 \\ T_{12} = 0 \\ T_{21} = 0 \end{cases}$$

which, taking into account (32), are solved for

$$\bar{T} = \begin{pmatrix} 1 & 0 \\ 0 & -1 \end{pmatrix} .$$

According to Proposition III.3, there is a one-on-one correspondence between the solutions of (27) generated by the constant forcing current I and those of (33) belonging to the invariant manifold

$$\mathcal{M}_{\mathcal{I}} = \Big\{ v_{C_m} \in \mathbb{R}, i_{L_m} \in \mathbb{R}, \varphi_M \in \mathbb{R} : \; C_m R_m v_{C_m} + L_m i_{L_m} + (1 - R_m)\, \varphi_M + \frac{R_m}{3} \varphi_M^3 = \mathcal{I} \Big\} , \quad (34)$$

with the manifold index given by

$$\mathcal{I} = \frac{c}{b} I .$$

Moreover, from Proposition III.2 and in particular from (13), it follows that the solution of (27) with initial conditions $V(t_0) = V_0$, $W(t_0) = W_0$ is reproduced by that of (33) with initial conditions

$$\begin{pmatrix} v_{C_m}(t_0) \\ i_{L_m}(t_0) \end{pmatrix} = z_0 = \begin{pmatrix} V_0 - W_0 - \dfrac{V_0^3}{3} + I \\ acW_0 - abV_0 \end{pmatrix} , \quad (35)$$
$$\varphi_M(t_0) = \varphi_{M_0} = V_0 .$$

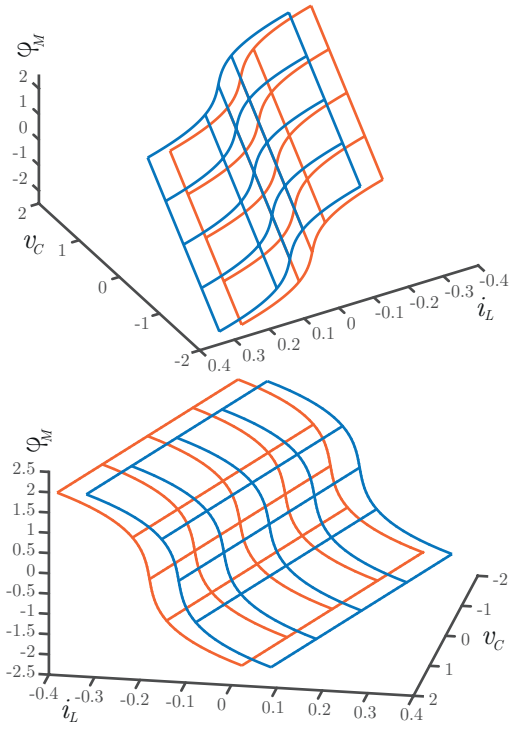

Figure 5. Two samples, observed from different points of view, of the invariant manifold (34) pertaining the FitzHugh-Nagumo circuit (33) for the parametric configuration (37). The upper surface corresponds to the manifold index $\mathcal{I} = 0.16$, while the lower one to index $\mathcal{I} = -0.64$.

A. *Numerical simulations*

Consider the FitzHugh-Nagumo model (27). Without any loss of generality, both the state variables and the time variable can be assumed to be expressed in normalized values, which are obtained from the corresponding biological values by shifting the axes origin and applying a scale factor. Then, consider the normalized parametric configuration

$$a = 0.2 , \qquad b = 0.4 , \qquad c = 0.32 , \quad (36)$$

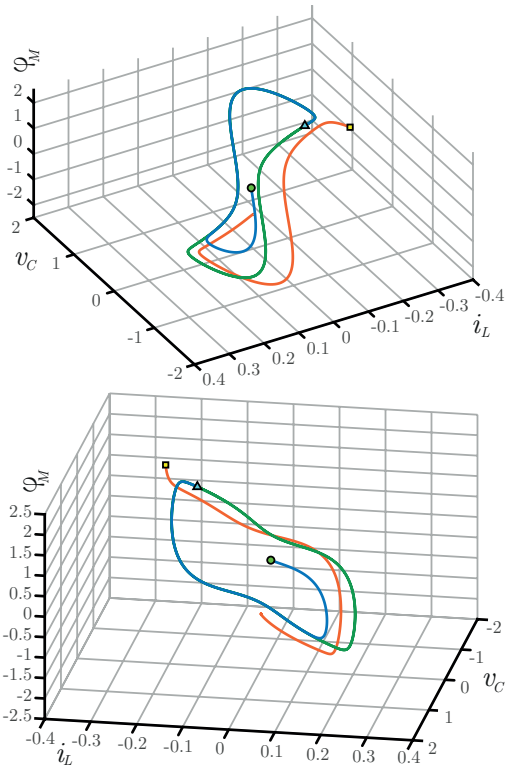

Figure 6. State space orbits of the FitzHugh-Nagumo circuit (33)-(37) originated from the initial conditions $x_0^{(1)}$, $x_0^{(2)}$, $x_0^{(3)}$ transformed according to (35). The circle, triangle and square correspond to the equivalent symbols used in Fig. 3 for the simulation of the FitzHugh-Nagumo system. The trajectories starting from the circle and triangle lie on the manifold of index $\mathcal{I} = 0.16$, while the orbit originated from the square lies onto the manifold of index $\mathcal{I} = -0.64$.

which is coherent with the original system (see [44], [45], [46]). The system is numerically simulated in the Matlab environment using the ode45 solver for different constant values of the input I and of the initial conditions x_0. Figure 3 depicts the trajectory obtained for input $I = 0.2$ starting from $x_0^{(1)} = (0.1, 0.4)^T$. For the sake of the next discussion, after 20 time units the simulation is stopped and the reached state is used as a new starting point $x_0^{(2)} = (1.8189, 0.0740)^T$ for a second run lasting other 80 time units. The corresponding trajectory is drawn with a different line style. The same figure shows also a different orbit originated from $x_0^{(3)} = (2, -1)^T$ when $I = -0.8$. Figure 4 illustrates the same trajectories in their temporal evolution.

Consider now the corresponding memristor circuit depicted in Fig. 2. From (32), the normalized equations of circuit (33) feature

$$R_m = 0.8\ , \qquad L_m = 12.5\ , \qquad C_m = 1\ . \tag{37}$$

In view of practical implementation, an impedance scaling technique has to be employed to obtain realistic values of the circuit components. The previous starting points $x_0^{(1)}$, $x_0^{(2)}$, $x_0^{(3)}$ are transformed via (35) into the initial conditions $(z_0^{(1)}, \varphi_{M_0}^{(1)})$, $(z_0^{(2)}, \varphi_{M_0}^{(2)})$, $(z_0^{(3)}, \varphi_{M_0}^{(3)})$. From (34) it follows that $(z_0^{(1)}, \varphi_{M_0}^{(1)})$ and $(z_0^{(2)}, \varphi_{M_0}^{(2)})$ belong to the same

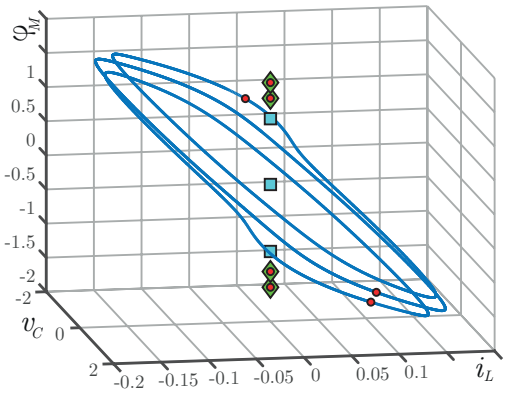

Figure 7. The FitzHugh-Nagumo circuit (33)-(37) exhibits a very rich dynamics comprising an infinite amount of different attractors according to the characterization illustrated in Section III. Seven different solutions are initialized so that their initial conditions (the circle symbols) are settled on different attractors. The diamonds and squares are, respectively, stable and unstable equilibrium points of the system, while the solid closed curves are stable limit cycles.

manifold of index $\mathcal{I} = 0.16$, while $(z_0^{(3)}, \varphi_{M_0}^{(3)})$ belongs to that of index $\mathcal{I} = -0.64$. A picture of the corresponding manifolds is provided by Fig. 5. The trajectories of the circuit originated from those starting points are shown in Fig. 6.

V. Extension to non-constant inputs u

In this section we relax the assumption that the input u of Σ is constant. We recall that Σ typically displays an attractor for many constant values of the input u, as illustrated in Fig. 7 for the FitzHugh-Nagumo model. Consider the case where Σ exhibits two different attractors for the input values $U_0^{(1)}$ and $U_0^{(2)}$, $U_0^{(1)} \neq U_0^{(2)}$, and let $u(t)$ be varied between these values in order to make the dynamics switching between the different attractors.

As an example, we can consider the input

$$u(t) = \begin{cases} U_0^{(1)} & \text{if} \quad t \in [t_0, t_1] \\ r(t) & \text{if} \quad t \in [t_1, t_2] \\ U_0^{(2)} & \text{if} \quad t \in [t_2, +\infty)\ , \end{cases} \tag{38}$$

where $r(t)$ satisfies $r(t_1) = U_0^{(1)}$ and $r(t_2) = U_0^{(2)}$. With some abuse of notation, we denote by $x^0(t)$ the solution with initial condition $x(t_0) = x_0$ and input u as in (38). We suppose that at $t = t_1$ such a solution lies onto the attractor corresponding to the constant input $U_0^{(1)}$, while at $t = t_2$ it belongs to the stability region of the attractor relative to the constant input $U_0^{(2)}$ so that it converges towards this attractor for $t > t_2$. Propositions III.2 and III.3 ensure that the attractors are replicated onto the two different invariant manifolds $\mathcal{M}_\mathcal{I}$ with $\mathcal{I} = -CA^{-1}DU_0^{(1)}$ and $\mathcal{I} = -CA^{-1}DU_0^{(2)}$. Clearly, the switching solution $x^0(t)$ cannot be reproduced by Σ_C since its dynamics cannot move from one invariant manifold to another. However, it can be shown that $x^0(t)$ can be replicated by introducing suitable voltage/current sources in the two-terminal element $\mathbf{L}$ which has been synthesized in the case of constant inputs. We recall that in this case the state space representation and the impedance are as in (21) and (22),

respectively, and that $T = \bar{T}$ in Proposition III.2. Proceeding as in [37], we replace each capacitor C_i with the same capacitor with in parallel a current source $I_i^{(s)}$, $i = 1, \dots, n_C$, and each inductor L_j with the same inductor with in series a voltage source $V_j^{(s)}$, $j = 1, \dots, n_L$. It follows that the state space representation of the so-modified $\mathbf{L}$ becomes

$$\begin{cases} \dot{\bar{z}}(t) = \bar{A}_L \bar{z}(t) + \bar{B}_L i_{\mathbf{L}}(t) + \Lambda^{-1}\Psi(t) \\ v_{\mathbf{L}}(t) = \bar{C}_L \bar{z}(t) \ , \end{cases} \tag{39}$$

where $\Psi \in \mathbb{R}^n$ is the vector of the voltage and current sources, i.e.,

$$\Psi = (I_1^{(s)}, \dots, I_{n_C}^{(s)}, V_1^{(s)}, \dots, V_{n_L}^{(s)})^\top \ , \tag{40}$$

and $\Lambda \in \mathbb{R}^{n \times n}$ is the following non-singular diagonal matrix

$$\Lambda = \text{diag } (C_1, \dots, C_{n_C}, L_1, \dots, L_{n_L}) \ . \tag{41}$$

Hence, by joining equations (39) with (5) and exploiting conditions (10) and (11), we get that the dynamics of the modified memristor circuit obeys

$$\begin{cases} \dot{\bar{z}}(t) = \bar{T}^{-1} A \bar{T} \bar{z}(t) + \bar{T}^{-1} B \dot{f}(\varphi_M(t)) + \Lambda^{-1}\Psi(t) \\ \dot{\varphi}_M(t) = C \bar{T} \bar{z}(t) \ . \end{cases} \tag{42}$$

The next result is instrumental for the design of the vector Ψ ensuring that equations (42) replicate the switching solution of Σ.

Proposition V.1. *Let $x^0(t)$ denote the solution of Σ with initial condition $x^0(t_0) = x_0$ and non-constant input $u(t)$ such that $\dot{u}(t)$ is piecewise-continuous for $t \geq t_0$, and let $\bar{z}^0(t)$ and $\varphi_M^0(t)$ be the solutions for $t \geq t_0$ of (42) with initial conditions*

$$z_0 = \bar{T}^{-1} \left(A x_0 + B f(C x_0) + D u(t_0) \right) \ , \ \varphi_{M_0} = C x_0 \ . \tag{43}$$

Suppose that the vector Ψ of the current and voltage sources satisfies

$$\Psi(t) = \Lambda \bar{T}^{-1} D \dot{u}(t) \tag{44}$$

for $t \geq t_0$. Then, $x^0(t)$ can be written as

$$x^0(t) = x_0 + \int_{t_0}^{t} \bar{T} \bar{z}^0(\tau) d\tau \ . \tag{45}$$

Proof. By proceeding as in the proof of Proposition III we have that the equations

$$\begin{cases} \dot{\xi}(t) = A \xi(t) + B \dot{f}(\eta(t)) + D \dot{u}(t) \\ \dot{\eta}(t) = C \xi(t) \end{cases} \tag{46}$$

admit the solutions $\xi(t) = \dot{x}^0(t)$ and $\eta(t) = C x^0(t)$ for the initial condition $\xi(t_0) = A x_0 + B f(C x_0) + D u(t_0)$ and $\eta(t_0) = C x_0$. We observe that equations (42) can be rewritten as

$$\begin{cases} \bar{T} \dot{\bar{z}}(t) = A \bar{T} \bar{z}(t) + B \dot{f}(\varphi_M(t)) + D \dot{u}(t) \\ \dot{\varphi}_M(t) = C \bar{T} \bar{z}(t) \end{cases} \tag{47}$$

once Ψ is replaced with its expression in (44). By comparing (47) and (46), it readily follows that the solutions $\bar{z}^0(t)$ and $\varphi_M^0(t)$ of (47) with the initial conditions in (43) are such that $\varphi_M^0(t) = C x^0(t)$ and $\bar{T} \bar{z}^0(t) = \dot{x}^0(t)$, thus proving (45). ■

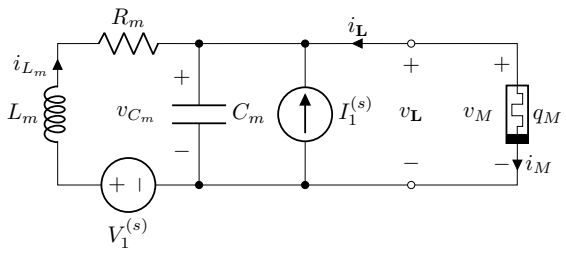

Figure 8. The memristor circuit designed to reproduce the FitzHugh-Nagumo dynamics for non-constant input I. The circuit might use up to two independent sources $I_1^{(s)}$ and $V_1^{(s)}$ to steer the state among the invariant manifolds, which characterize the state space when the input I of the original dynamics (27) is assumed constant.

Remark 4. *It is worth noting that if $u(t)$ is as in* (38) *then $u(t_0) = U_0^{(1)}$, $u(t_2) = U_0^{(2)}$ and $\Psi(t) = 0$ for both $t \in [t_0, t_1]$ and $t > t_2$. According to Proposition III, this implies that the solutions $\bar{z}^0(t)$ and $\varphi_M^0(t)$ of (42) is confined to lie onto the invariant manifold*

$$\mathcal{M}_{\mathcal{I}} = \big\{ \bar{z} \in \mathbf{R}^n, \varphi_M \in \mathbb{R} : \\ \varphi_M - C A^{-1} \bar{T} \bar{z} + C A^{-1} B f(\varphi_M) = \mathcal{I} \big\} \ ,$$

with $\mathcal{I} = -C A^{-1} D U_0^{(1)}$ for $t \in [t_0, t_1]$ and $\mathcal{I} = -C A^{-1} D U_0^{(2)}$ for $t \geq t_2$. Since for $t \in [t_1, t_2]$ the input $u(t)$ is non-constant, $\bar{z}^0(t)$ and $\varphi_M^0(t)$ are not belonging to any invariant manifold. This means that the manifold index

$$\mathcal{I} = \varphi_M - C A^{-1} \bar{T} \bar{z} + C A^{-1} B f(\varphi_M)$$

is no longer constant. In fact, we have

$$\begin{aligned} \dot{\mathcal{I}}(t) &= \dot{\varphi}_M^0(t) - C A^{-1} \bar{T} \dot{\bar{z}}^0(t) + C A^{-1} B \dot{f}(\varphi_M^0(t)) \\ &= -C A^{-1} D \dot{u}(t) \end{aligned} \tag{48}$$

where the second equality follows by replacing $\bar{T} \dot{\bar{z}}^0(t)$ and $\dot{\varphi}_M^0(t)$ with the expressions in the right-side terms of (47), respectively. Since $\mathcal{I}(t_0) = -C A^{-1} D u(t_0)$, from (48) we get

$$\mathcal{I}(t) = -C A^{-1} D u(t) \ . \tag{49}$$

Hence, for $t \in [t_1, t_2]$ the index of the manifold varies linearly with the non-constant input of Σ.

A. The FitzHugh-Nagumo model

According to the above results, the implementation of the memristor circuit when input u is non-constant is achieved by introducing as many voltage and current sources as the number of inductors and capacitors, respectively, in the circuit implementation already obtained for the constant input case. Taking into account that all the voltage sources must be in series of the inductors, and the current sources in parallel of the capacitors, the application of this procedure to the circuit equations (33) brings to the circuit implementation illustrated in Fig. 8, which is described by the following system:

$$\begin{cases} \dot{v}_{C_m} = \dfrac{1}{C_m} \left(i_{L_m} + (1 - \varphi_M^2) v_{C_m} + I_1^{(s)} \right) \\ \dot{i}_{L_m} = -\dfrac{1}{L_m} \left(v_{C_m} + R_m i_{L_m} - V_1^{(s)} \right) \\ \dot{\varphi}_M = v_{C_m} \end{cases} \ . \tag{50}$$

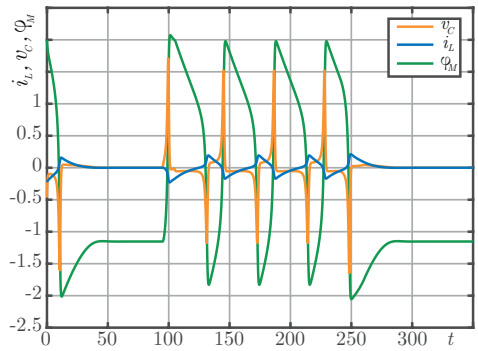

Figure 9. Time representation of the solution of the FitzHugh-Nagumo circuit described in Subsection V-A. During the intervals $(95, 105)$, $(240, 260)$ the manifold index is changed from $\mathcal{I} = -0.64$ to $\mathcal{I} = 0.36$ and back to $\mathcal{I} = -0.64$ using the current source.

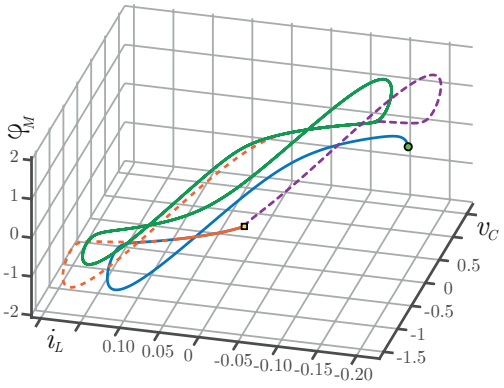

Figure 10. State space orbits of the FitzHugh-Nagumo circuit described in Subsection V-A. The trajectory starts from a stable fixed point (the circle symbol) in the manifold of index $\mathcal{I} = -0.64$, then the system is brought onto the manifold of index $\mathcal{I} = 0.36$, where a stable limit cycle attracts the trajectory, and, finally, it is switched back to $\mathcal{I} = -0.64$, where it lands onto the starting equilibrium point. Lines are solid when the dynamics evolves onto a manifold, i.e., when the manifold index is constant, while they are dashed during the passage from a manifold to another.

Observe that the vector of the sources is $\Psi = (I_1^{(s)}, V_1^{(s)})^\top$, just in agreement with (40). Also, note that $\Lambda = \text{diag}\,(C_m, L_m)$ in accordance to (41). In order to change the manifold index as in (49), condition (44) must be enforced. Taking into account (32), it turns out that

$$\Psi(t) = \begin{pmatrix} I_1^{(s)}(t) \\ V_1^{(s)}(t) \end{pmatrix} = \begin{pmatrix} C_m \\ 0 \end{pmatrix} \dot{u}(t) \ .$$

Therefore, the voltage source $V_1^{(s)}$ is not necessary to steer the manifold index. From (49) it follows that such a Ψ enforces in the manifold index the following dynamics:

$$\mathcal{I}(t) = \frac{c}{b} u(t) = R_m u(t) \ ,$$

where u stands for the time-varying stimulus of the FitzHugh-Nagumo system, as described by (28)-(29). Note that its derivative $\dot{u}$ is the real objective of the design, since it defines the actual implementation of the current source, that, in this

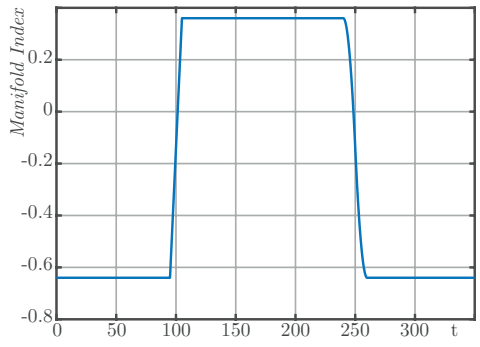

Figure 11. Evolution of the manifold index of the FitzHugh-Nagumo circuit described in Subsection V-A. The index switches between the values $\mathcal{I} = -0.64$ and $\mathcal{I} = 0.36$. During the interval $(95, 105)$ it increases as a linear ramp, while in $(240, 260)$ it decreases as a parabolic ramp, according to the programming of the current source.

example, has been chosen as follows:

$$I_1^{(s)}(t) = \begin{cases} 0 \ , & t \in [0, 95] \\ 0.1 \dfrac{C_m}{R_m} \ , & t \in (95, 105) \\ 0 \ , & t \in [105, 240] \\ -4C_m \dfrac{t - 240}{20^2 R_m} \ , & t \in (240, 250) \\ -4C_m \dfrac{260 - t}{20^2 R_m} \ , & t \in [250, 260) \\ 0 \ , & t \in [260, +\infty) \ . \end{cases}$$

In Fig. 9 the circuit (50) is numerically simulated, as before, by the Matlab software, and the same configuration (37) used in Section IV-A is considered. The manifold index (or equivalently u) is kept constant over the time intervals $[0, 95]$, $[105, 240]$, and $[260, 350]$, so that during these periods the circuit dynamics remains confined into three different invariant manifolds respectively of indexes $\mathcal{I} = -0.64$, $\mathcal{I} = 0.36$, and again $\mathcal{I} = -0.64$, which in the original FitzHugh-Nagumo system correspond to $I = -0.8$ and $I = 0.2$. During the transients $(95, 105)$ and $(240, 260)$, the $I_1^{(s)}$ source (or equivalently $\dot{u}$) is used to steer the trajectory from a manifold to another. In particular, it is constant and non-negative in $(95, 105)$ and it acts as a linear ramp in $(240, 260)$. Therefore, the manifold index varies as linear ramp in the first period, and as a decreasing parabolic ramp in the second one. Out of these intervals the source is constant at zero, and therefore the manifold index remains unchanged. Figure 10 illustrates the same resulting trajectory in the state space of the circuit, while the dynamics of the manifold index is reported in Fig. 11.

B. The Duffing system

The application of the previous results will be illustrated by designing a memristor circuit capable to reproduce the dynamics of the forced Duffing system. Other memristive Duffing type circuits have been proposed in the recent literature (see, e.g., [52], [53]), but their design has been mainly inspired

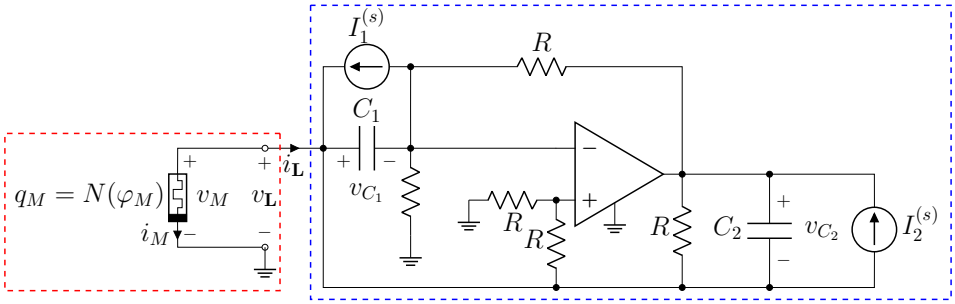

Figure 12. Memristor circuit reproducing the dynamics of the Duffing system (51): the active two-terminal element $\mathbf{L}$ (blue box), designed via the technique in [43] with R, C_1, and C_2 as in (55), and the flux-controlled memristor (red box) with the nonlinear characteristic (54).

by the original nonlinear circuit [54]. The Duffing system equation reads [55]

$$\ddot{\xi}(t) + \delta\dot{\xi}(t) + \alpha\xi + \beta\xi^3(t) = u(t) \ , \tag{51}$$

where the forcing input $u(t)$ is any non-constant input satisfying the assumptions of Proposition V.1. System (51) can be put in form (1) by defining

$$\begin{aligned} &x = \begin{pmatrix} \xi \\ \dot{\xi} \end{pmatrix} \ , \ f(y) = -y^3 \ , \ A = \begin{pmatrix} 0 & 1 \\ -\alpha & -\delta \end{pmatrix} \ , \\ &B = \begin{pmatrix} 0 \\ \beta \end{pmatrix} \ , \ C = \begin{pmatrix} 1 & 0 \end{pmatrix} \ , \ D = \begin{pmatrix} 0 \\ 1 \end{pmatrix} \end{aligned} \tag{52}$$

and the corresponding $L(s)$ is

$$L(s) = \frac{\beta}{s^2 + \delta s + \alpha} \ .$$

For the implementation's sake and without any loss of generality, consider the equivalent though extended form (24), where k plays the role of an additional degree of freedom. Then, the synthesis of the circuit can be performed starting from impedance (25), which turns out equal to

$$L_k(s) = \frac{\beta}{s^2 + \delta s + \alpha + k\beta} \ . \tag{53}$$

Indeed, if $\alpha + k\beta > 0$, the impedance (53) can be obtained via the circuit $\mathbf{L}$ depicted in Fig. 12, where each capacitor has already been coupled with as many parallel current sources.

The equations governing the two-terminal element $\mathbf{L}$ are

$$\begin{cases} \dot{v}_{C_1} = -\dfrac{1}{RC_1} v_{C_2} + \dfrac{1}{C_1} I_{g_1} \\ \dot{v}_{C_2} = \dfrac{1}{RC_2} v_{C_1} - \dfrac{2}{RC_2} v_{C_2} + \dfrac{1}{C_2} I_{g_2} - \dfrac{1}{C_2} i_{\mathbf{L}} \\ v_{\mathbf{L}} = 2 v_{C_1} \end{cases}$$

and, thus, they admit the form (39) once $\bar{z} = (v_{C_1}, v_{C_2})^\top$ and

$$\bar{A}_L = \begin{pmatrix} 0 & -\dfrac{1}{RC_1} \\ \dfrac{1}{RC_2} & -\dfrac{2}{RC_2} \end{pmatrix}, \bar{B}_L = \begin{pmatrix} 0 \\ -\dfrac{1}{C_2} \end{pmatrix},$$

$$\bar{C}_L = \begin{pmatrix} 2 & 0 \end{pmatrix}, \Lambda = \begin{pmatrix} C_1 & 0 \\ 0 & C_2 \end{pmatrix}, \Psi(t) = \begin{pmatrix} I_1^{(s)}(t) \\ I_2^{(s)}(t) \end{pmatrix}.$$

The complete circuit is obtained by introducing the dynamics (5) of the memristor $\mathbf{MR}$ with

$$N(y) = -f_k(y) = -f(y) - ky = y^3 - ky \ . \tag{54}$$

The solution of (23) leads to

$$\begin{aligned} &R = \frac{\beta}{2(\alpha + k\beta)} \ , \ C_1 = \frac{\delta}{\beta} \ , \ C_2 = \frac{4(\alpha + k\beta)}{\beta\delta} \ , \\ &\bar{T} = \begin{pmatrix} 2 & 0 \\ 0 & -\dfrac{2}{RC_1} \end{pmatrix} \ , \end{aligned} \tag{55}$$

and also to the inverse relationships between the circuit elements and the original dynamics' parameters, which are

$$\alpha = \frac{1 - 2kR}{R^2 C_1 C_2} \ , \quad \beta = \frac{2}{RC_1 C_2} \ , \quad \delta = \frac{2}{RC_2} \ .$$

Finally, observe that equation (44) gives

$$\Psi(t) = \begin{pmatrix} 0 \\ -\dfrac{1}{2} RC_1 C_2 \end{pmatrix} \dot{u}(t) \ ,$$

and then the current source $I_1^{(s)}$ turns out unnecessary. Indeed, the manifold index is related to the input u as follows:

$$\begin{aligned} \mathcal{I}(t) = & -C(A - kBC)^{-1} D u(t) = R^2 C_1 C_2 u(t) \\ = & \frac{1}{\alpha + k\beta} u(t) \ . \end{aligned} \tag{56}$$

The Duffing system (51) in its state representation (52) has been numerically simulated in the Matlab environment for different inputs $u(t)$ when the parametric configuration is $\alpha = -1$, $\beta = 1$, $\delta = 0.3$. Figures 13.A, 13.B, and 13.C shows the trajectories generated from $x_0^{(1)} = (-0.4881, 0.3745)^\top$, $x_0^{(2)} = (-0.3669, 0.3592)^\top$, and $x_0^{(3)} = (-0.7809, 0.4658)^\top$, when $u(t)$ is equal $u_1(t) = 0.25\cos(1.2t)$, $u_2(t) = 0.28\cos(1.2t)$, and $u_3(t) = 0.29\cos(1.2t)$, respectively. As the input amplitude increases, Duffing system exhibits a limit cycle undergoing a period doubling cascade, which ends into chaos. The chaotic attractor for $u_4(t) = 0.50\cos(1.2t)$ is reported in Fig. 13.D for the initial condition $x_0^{(4)} = (-0.8553, 0.5371)^\top$. According to (55) and assuming $k = 2$ so that $\alpha + k\beta = 1$, the corresponding memristor circuit features the parameters $R = 0.5$, $C_1 = 0.3$, $C_2 = 13.3333$. The starting points of the simulations of Fig.s 13.A, 13.B, 13.C,

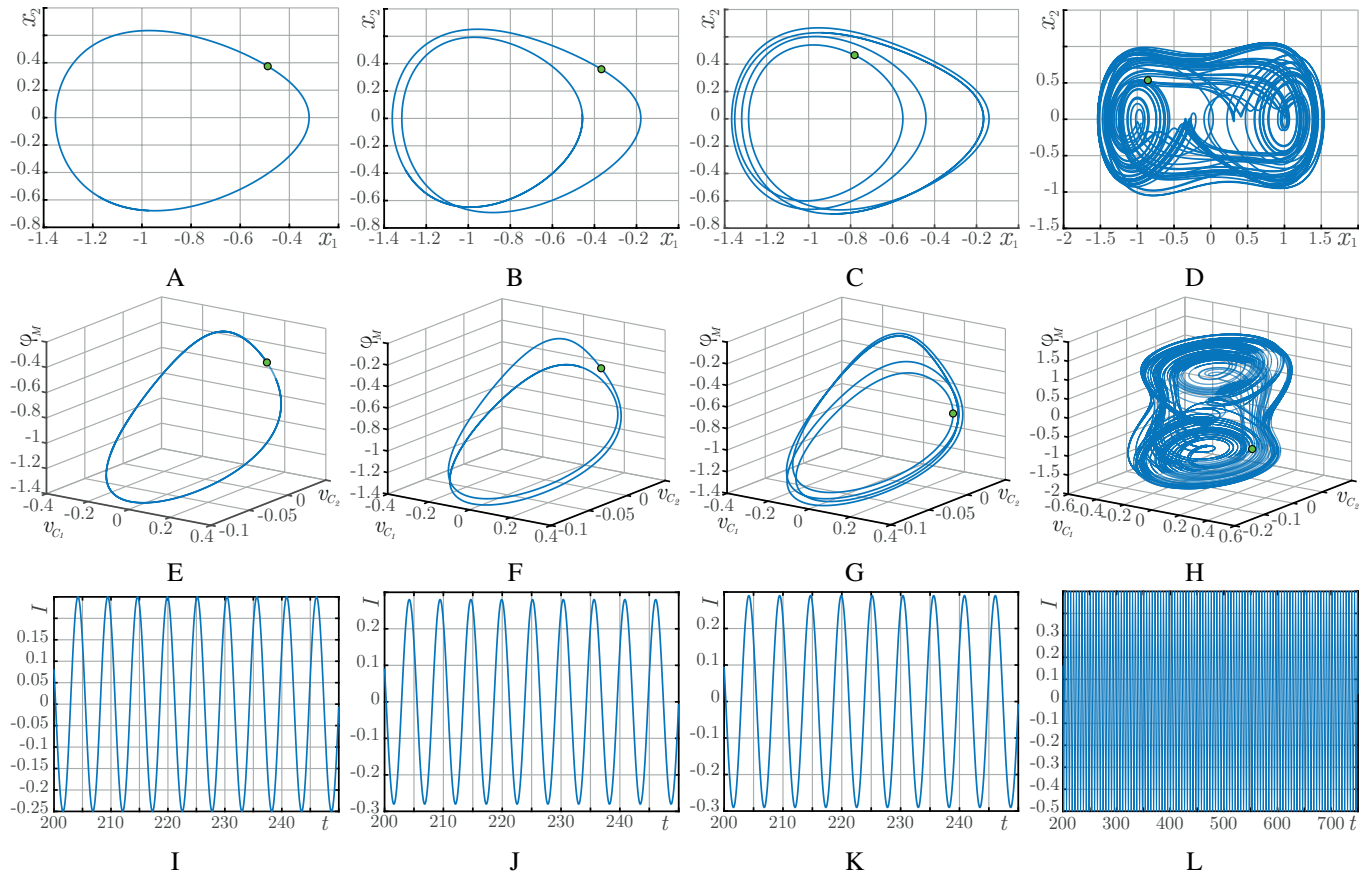

Figure 13. First row: Different dynamics exhibited by the Duffing system (51) in its state representation (52). A, B, C, D: State space orbits originated from $x_0^{(1)}$, $x_0^{(2)}$, $x_0^{(3)}$, and $x_0^{(4)}$ (the circle symbols) when the system if respectively forced by $u_1(t)$, $u_2(t)$, $u_3(t)$, and $u_4(t)$. Second row: Different dynamics exhibited by the Duffing circuit of Fig. 12 for configurations equivalent to those reported in the left column for the Duffing system. E, F, G, H: State space orbits of originated from the initial conditions (57) computed on the couples $(x_0^{(1)}, u_1(t_0))$, $(x_0^{(2)}, u_2(t_0))$, $(x_0^{(3)}, u_3(t_0))$, and $(x_0^{(4)}, u_4(t_0))$ derived from the original configurations of the Duffing system. In each case the circuit is driven by the related $I_2^{(s)}(t)$. Third row: Behavior of the manifold index (56) for the Duffing circuit of Fig. 12 when it is configured as in the scenarios of the center column. I, J, K, L: Temporal evolution of the manifold index under the forcing input $I_2^{(s)}(t)$.

and 13.D are transformed into initial conditions of the circuit according to (43), which reads

$$z_0 = \begin{pmatrix} \frac{1}{2}x_{0,2} \\ \frac{\delta}{4(\alpha+k\beta)}\left(\alpha x_{0,1} + \delta x_{0,2} + \beta x_{0,1}^3 - u_0\right) \end{pmatrix} \quad (57)$$

$$\varphi_{M_0} = x_{0,1} \ ,$$

where $x_{0,i}$ denotes the i-th element of vector x_0, and $u_0 = u(t_0) = \gamma\cos(1.2t_0)$ for $\gamma \in \{0.25, 0.28, 0.29, 0.50\}$, depending on the chosen input. The corresponding simulations are illustrated in Fig.s 13.E, 13.F, 13.G, and 13.H. The dynamics of the corresponding manifold indexes, instead, has been reported in Fig.s 13.I, 13.J, 13.K, and 13.L. Figures 13.H and 13.L show the behaviors of the circuit state and of the index, which correspond to the chaotic orbit described in the situation of Fig. 13.D.

VI. Extension to Charge-Controlled Memristors

In this section we consider the case when the memristor **MR** in Fig. 1 is assumed to be an ideal charge-controlled memristor. Such a memristor is described by a nonlinear

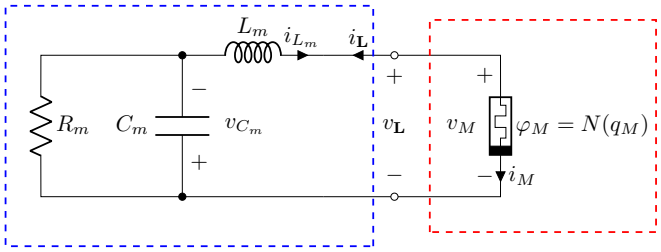

Figure 14. Memristor circuit capable to reproduce the dynamics of the FitzHugh-Nagumo neuron model with a charge-controlled memristor (red box) of nonlinear characteristic (60) and a passive two-terminal elementi **L** (blue box) with R_m, L_m, and C_m as in (61).

charge-flux characteristic which is denoted by $N(\cdot)$ as in the case of the flux-controlled memristor. It relates the memristor charge and flux as follows

$$\varphi_M = N(q_M) \ .$$

In the voltage-current domain the memristor dynamics is modeled by the following nonlinear system

$$\mathbf{MR}: \begin{cases} \dot{q}_M(t) = i_M(t) \\ v_M(t) = \dot{N}(q_M(t)) = N'(q_M(t))i_M(t) \end{cases}, \tag{58}$$

where the derivative $N'(q_M)$ is known as the memristance of the memristor.

Note that in the case of charge-controlled memristor i_M and v_M are the input and the output of $\mathbf{MR}$, respectively. Hence, to ensure that the memristor circuit of Fig. 1 is well-posed, the two-terminal element $\mathbf{L}$ should have $v_{\mathbf{L}}$ as input and $i_{\mathbf{L}}$ as output, i.e., $\mathbf{L}$ is either a passive or an active input-less circuit which is described by the following state space representation

$$\mathbf{L}: \begin{cases} \dot{z}(t) = A_L z(t) + B_L v_{\mathbf{L}}(t) \\ i_{\mathbf{L}}(t) = C_L z(t) \end{cases},$$

where $z \in \mathbb{R}^n$, $A_L \in \mathbb{R}^{n\times n}$, $B_L \in \mathbb{R}^{n\times 1}$, $C_L \in \mathbb{R}^{1\times n}$. Observe that in this case the strictly proper rational function

$$L(s) = C_L(sI_n - A_L)^{-1}B_L ,$$

is the admittance of the two-terminal element.

Since $v_{\mathbf{L}} = v_M$ and $i_{\mathbf{L}} = -i_M$, it follows that the dynamics of the circuit of Fig. 1 obeys the following equations

$$\Sigma_C: \begin{cases} \dot{z}(t) = A_L z(t) - B_L \dot{N}(q_M(t)) \\ \dot{q}_M(t) = C_L z(t) \end{cases}, \tag{59}$$

which have been labeled with the same symbol Σ_C used for the equations (6) in the flux-controlled memristor case.

By comparing (6) and (59) we note that the unique difference is that φ_M has been replaced with q_M. Hence, we can conclude that all the results obtained for the flux-controlled memristor are still valid for the case of the charge-controlled memristor, once the flux φ_M is replaced by the charge q_M. Clearly, now $\mathbf{L}$ should be synthesized by ensuring that its admittance is equal to (4).

A. The charge-controlled FitzHugh-Nagumo circuit

In this subsection a charge-controlled memristor circuit is derived for the FitzHugh-Nagumo neuron model by following the previous procedure. In this case, the memristor is described by (58) along with the nonlinear characteristic

$$N(q_M) = -q_M + \frac{q_M^3}{3} , \tag{60}$$

while $L(s)$ in (31) represents the admittance of the two-terminal element $\mathbf{L}$ between $v_{\mathbf{L}}$ and $i_{\mathbf{L}}$. This implies that the corresponding impedance can be written as

$$L^{-1}(s) = \frac{s^2 + acs + ab}{s + ac} = s + \frac{ab}{s + ac} .$$

Hence, it turns out that it can be synthesized by the series of an inductor L_m with the parallel connection of a resistor R_m and a capacitor C_m, once

$$R_m = \frac{b}{c} , \qquad L_m = 1 , \qquad C_m = \frac{1}{ab} . \tag{61}$$

Figure 14 depicts the implemented circuit which is governed by the following equations

$$\begin{cases} \dot{v}_{C_m} = -\dfrac{1}{R_m C_m} v_{C_m} - \dfrac{1}{C_m} i_{L_m} \\ \dot{i}_{L_m} = -\dfrac{1}{L_m} v_{C_m} - \dfrac{1}{L_m} v_M \\ \dot{q}_M = i_M \end{cases}, \tag{62}$$

where $v_M = \dot{N}(q_M)$ and $i_M = -i_{L_m}$. Since $v_{\mathbf{L}} = v_M$ and $i_{\mathbf{L}} = -i_{L_m}$, we get that (62) can be written as in (6) once $z = (v_{C_m}, i_{L_m})^\top$ and $A_L = \bar{A}_L$, $B_L = \bar{B}_L$, $C_L = \bar{C}_L$ with

$$\bar{A}_L = \begin{pmatrix} -\dfrac{1}{R_m C_m} & -\dfrac{1}{C_m} \\ \dfrac{1}{L_m} & 0 \end{pmatrix} , \quad \bar{B}_L = \begin{pmatrix} 0 \\ -\dfrac{1}{L_m} \end{pmatrix} ,$$
$$\bar{C}_L = \begin{pmatrix} 0 & -1 \end{pmatrix} .$$

Finally, the matrix $\bar{T}$ solving conditions (23) is

$$\bar{T} = \begin{pmatrix} 0 & -1 \\ 1 & 0 \end{pmatrix} .$$

VII. Conclusions

In this paper the dynamics of a class of forced nonlinear systems which includes several systems displaying complex dynamics, has been considered. First, it has been shown that there exists a one-to-one correspondence between the dynamics of the nonlinear system obtained for a given constant value of the forcing input and that displayed on one of the invariant manifolds of a suitably synthesized input-less circuit composed of a two-terminal element connected with an ideal flux-controlled memristor. In particular, it turns out that in the case of the FitzHugh-Nagumo model there is a linear relation between the values of the injected current and the index of the invariant manifolds. Then, it is shown that, even in the case of a non-constant forcing input, the system dynamics can be still replicated by introducing suitably programmed voltage/current sources in the two-terminal element of the circuit, as illustrated via the application to the FitzHugh-Nagumo model and the Duffing system. Also, it is observed that quite similar results hold if the flux-controlled memristor is replaced by a charge-controlled one. Several future research issues can be foreseen, such as the practical implementation of ideal memristor and their interconnection with suitably designed two-terminal elements, as well as the study of the capability of circuits with real physical memristors to replicate the dynamics of known oscillatory systems.

Acknowledgment

This work was supported by the project "Analogue COmputing with Dynamic Switching Memristor Oscillators: Theory, Devices and Applications (COSMO)," Grant PRIN 2017LSCR4K 002, funded by the Italian Ministry of Education, University and Research (MIUR).

REFERENCES

[1] M. M. Waldrop. The chips are down for Moore's law. *Nature News*, 530(7589):144, 2016.

[2] M. A. Zidan, J. P. Strachan, and W. D. Lu. The future of electronics based on memristive systems. *Nature Electronics*, 1(1):22, 2018.

[3] D. Ielmini and H. S. P. Wong. In-memory computing with resistive switching devices. *Nature Electronics*, 1(6):333–343, 2018.

[4] O. Krestinskaya, A. P. James, and L. O. Chua. Neuromemristive circuits for edge computing: A review. *IEEE Trans. Neural Netw. Learn. Syst.*, pages 1–20, 2019.

[5] L. O. Chua. Memristor-The missing circuit element. *IEEE Trans. Circuit Theory*, 18(5):507–519, 1971.

[6] L. O. Chua and S. M. Kang. Memristive devices and systems. *Proc. IEEE*, 64(2):209–223, 1976.

[7] L. Chua. Everything you wish to know about memristors but are afraid to ask. *Radioengineering*, 24(2):319–368, 2015.

[8] B. Hajri, H. Aziza, M. M. Mansour, and A. Chehab. RRAM device models: A comparative analysis with experimental validation. *IEEE Access*, 7:168963–168980, 2019.

[9] P. Y. Chen and S. Yu. Compact modeling of RRAM devices and its applications in 1T1R and 1S1R array design. *IEEE Trans. Electron Devices*, 62(12):4022–4028, 2015.

[10] P. Mazumder, S. M. Kang, and R. Waser (Eds.). Special issue on memristors: devices, models, and applications. *Proc. IEEE*, 100(6), Jun. 2012.

[11] F. Corinto and M. Forti. Memristor circuits: Flux-charge analysis method. *IEEE Trans. Circuits Syst. I: Reg. Papers*, 63(11):1997–2009, 2016.

[12] F. Corinto, M. Forti, and L. O. Chua. *Nonlinear Circuits and Systems with Memristors*. Springer, 2021.

[13] L. Chua, G. Sirakoulis, and A. Adamatzky (Eds.). *Handbook of Memristor Networks. Vol. 1 and 2*. Springer, New York, 2019.

[14] R. Tetzlaff (Ed.), *Memristors and Memristive Systems*. Springer, New York, 2014.

[15] J. A. Tuszynski, D. Friese, H. Freedman, V. I. Sbitnev, H. Kim, I. Santelices, A. P. Kalra, S. D. Patel, Sahil, K. Shankar, L. O. Chua. Microtubules as sub-cellular memristors. *Scientific reports*, 10(1):1–11, 2020.

[16] G. Chen, S. Ivanov, S. Urazhdin. Ideal memristor based on viscous magnetization dynamics driven by spin torque. *Applied Physics Letters*, 117(10):103501, 2020.

[17] T. Fu, X. Liu, H. Gao, J. E. Ward, X. Liu, B. Yin, Z. Wang, Y. Zhuo, D. J. F. Walker, J. Yang et al. Bioinspired bio-voltage memristors. *Nature communications*, 11(1):1–10, 2020.

[18] J. Secco, F. Corinto, and A. Sebastian. Flux–charge memristor model for phase change memory. *IEEE Transactions on Circuits and Systems II: Express Briefs*, 65(1):111–114, 2017.

[19] M.M. Al Chawa, R. Picos, J.B. Roldan, F. Jimenez-Molinos, M.A. Villena, and C. de Benito, Exploring resistive switching-based memristors in the charge–flux domain: A modeling approach. *International Journal of Circuit Theory and Applications*, 46(1), 29–38, 2018.

[20] J. Vista and A. Ranjan. A simple floating MOS-memristor for high-frequency applications. *IEEE Trans. Very Large Scale Integration (VLSI) Syst.*, 27(5):1186–1195, 2019.

[21] E. Solan and K. Ochs. Wave digital emulation of general memristors. *Int. J. Circuit Theory Appl.*, 46(11):2011–2027, 2018.

[22] A. Ascoli, F. Corinto, V. Senger, and R. Tetzlaff. Memristor model comparison. *IEEE Circuits Syst. Mag.*, 13(2):89–105, 2013.

[23] B. Bao, T. Jiang, Q. Xu, M. Chen, H. Wu, and Y. Hu. Coexisting infinitely many attractors in active band-pass filter-based memristive circuit. *Nonlinear Dynamics*, 86(3):1711–1723, 2016.

[24] C. Chen, J. Chen, H. Bao, M. Chen, and B. Bao. Coexisting multi-stable patterns in memristor synapse-coupled Hopfield neural network with two neurons. *Nonlinear Dynamics*, 95(4):3385–3399, 2019.

[25] H. Chang, Y. Li, F. Yuan, and G. Chen. Extreme multistability with hidden attractors in a simplest memristor-based circuit. *Int. J. Bifurcat. Chaos*, 29(06):1950086, 2019.

[26] F. Corinto and M. Forti. Memristor circuits: Bifurcations without parameters. *IEEE Trans. Circuits Syst. I, Reg. Papers*, 64(6):1540–1551, 2017.

[27] A. Amador, E. Freire, E. Ponce, and J. Ros. On discontinuous piecewise linear models for memristor oscillators. *Int. J. Bifurcat. Chaos*, 27(06):1730022, 2017.

[28] M. Messias, C. Nespoli, and V. A. Botta. Hopf bifurcation from lines of equilibria without parameters in memristor oscillators. *Int. J. Bifurcat. Chaos*, 20(02):437–450, 2010.

[29] J. Zhang and X. Liao. Effects of initial conditions on the synchronization of the coupled memristor neural circuits. *Nonlinear Dynamics*, 95(2):1269–1282, 2018.

[30] M. Di Marco, M. Forti, G. Innocenti, and A. Tesi. Harmonic balance method to analyze bifurcations in memristor oscillatory circuits. *International Journal of Circuit Theory and Applications*, 46(1):66–83, 2018.

[31] G. Innocenti, M. Di Marco, M. Forti, and A. Tesi. Prediction of period doubling bifurcations in harmonically forced memristor circuits. *Nonlinear Dynamics*, 96(2):1169–1190, 2019.

[32] G. Innocenti, M. Di Marco, A. Tesi, and M. Forti. Input–output characterization of the dynamical properties of circuits with a memelement. *Int. J. Bifurcation Chaos*, 30(07):2050110, 2020.

[33] F. Corinto and M. Forti. Memristor circuits: Pulse programming via invariant manifolds. *IEEE Trans. Circuits Syst. I, Reg. Papers*, 65(4):1327—1339, 2018.

[34] M. Chen, M. Sun, B. Bao, H. Wu, Q. Xu, and J. Wang. Controlling extreme multistability of memristor emulator-based dynamical circuit in flux–charge domain. *Nonlinear Dynamics*, 91(2):1395–1412, 2018.

[35] H. Bao, T. Jiang, K. Chu, M. Chen, Q. Xu, and B. Bao. Memristor-based canonical Chua's circuit: Extreme multistability in voltage-current domain and its controllability in flux-charge domain. *Complexity*, 2018, 2018.

[36] M. Di Marco, M. Forti, F. Corinto, and L. O. Chua. Unfolding nonlinear dynamics in analogue systems with mem-elements. *IEEE Transactions on Circuits and Systems I: Regular Papers*, 68(1):14–24, 2021.

[37] M. Di Marco, G. Innocenti, A. Tesi and M. Forti. Circuits with a mem-element: Invariant manifolds control via pulse programmed sources. *Nonlinear Dynamics*, 106:2577–2606, 2021.

[38] A. Ascoli, A.S. Demirkol, R. Tetzlaff, and L. Chua. Edge of Chaos Theory Resolves Smale Paradox. *IEEE Transactions on Circuits and Systems I: Regular Papers*, 69(3):1252-1265, 2022.

[39] A. Ascoli, A.S. Demirkol, R. Tetzlaff, and L. Chua. Edge of Chaos Is Sine Qua Non for Turing Instability. *IEEE Transactions on Circuits and Systems I: Regular Papers*,(in press) 2022.

[40] C. Du, F. Cai, M. A. Zidan, W. Ma, S. H. Lee, and W. D. Lu. Reservoir computing using dynamic memristors for temporal information processing. *Nature Comm.*, 8(1):2204, 2017.

[41] M. W. Hirsch. Convergent activation dynamics in continuous time networks. *Neural Netw.*, 2(5), 331–349, 1989.

[42] I. W. Sandberg, Synthesis of driving-point impedance with active RC-networks. *Bell Syst. Tech. J.*, 39:947–962, 1960.

[43] P. Horn, and G. Moschytz, Active RC single-opamp design of driving-point impedances. *IEEE Trans. Circuits Syst.*, 26(1):22—30, 1979.

[44] R. Fitzhugh. Impulses and physiological states in theoretical models of nerve membrane. *Biophys J*, 1(6):445–466, 1961.

[45] J. Nagumo, S. Arimoto, S. Yoshizawa. An active pulse transmission line simulating nerve axon. *Proc Ire*, 50(10):2061–70, 1962.

[46] E. M. Izhikevich. Dynamical Systems in Neuroscience: The Geometry of Excitability and Bursting. The MIT Press, Cambridge, MA, 2007.

[47] C. Rocsoreanu, A. Georgescu, and N. Giurgiteanu. The FitzHugh-Nagumo Model: Bifurcation and Dynamics. Kluwer Academic Publishers, Boston, 2000.

[48] A. L. Hodgkin, and A. F. Huxley. A quantitative description of membrane current and its application to conduction and excitation in nerve. *The Journal of physiology*, 117(4):500–544, 1952.

[49] H. Bao, W. Liu, and M. Chen. Hidden extreme multistability and dimensionality reduction analysis for an improved non-autonomous memristive FitzHugh–Nagumo circuit. *Nonlinear Dynamics*, 96:1879–1894, 2019.

[50] H. Handa, and B. B. Sharma. Synchronization of a set of coupled chaotic FitzHugh–Nagumo and Hindmarsh–Rose neurons with external electrical stimulation. *Nonlinear Dynamics*, 85(3):1517–1532, 2016.

[51] J. H. Zhang, and X. F. Liao. Synchronization and chaos in coupled memristor-based FitzHugh–Nagumo circuits with memristor synapse. *AEÜ Int. J. Electron. Commun.*, 75:82–90, 2017.

[52] K. Srinivasan, V. K. Chandrasekar, A. Venkatesan, and I. R. Mohamed. Duffing–van der Pol oscillator type dynamics in Murali–Lakshmanan–Chua (MLC) circuit. *Chaos, Solitons & Fractals*, 82:60–71, 2016.

[53] S. Sabarathinam, C. K. Volos, and K. Thamilmaran. Implementation and study of the nonlinear dynamics of a memristor-based Duffing oscillator. *Nonlinear Dynamics*, 87(1):37–49, 2017.

[54] K. Murali, and M. Lakshmanan. Transmission of signals by synchronization in a chaotic Van der Pol–Duffing oscillator. *Physical Review E*, 48(3):R1624, 1993.

[55] P. J. Holmes, and D. A. Rand. The bifurcations of Duffing's equation: An application of catastrophe theory. *Journal of Sound and Vibration*, 44(2):237–253, 1976.

G. Innocenti graduated in 2004 with a Master's Degree in Information Engineering at the University of Florence (Firenze, Italy), and from the same institution received the Ph.D. in Nonlinear Dynamics and Complex Systems in 2008. He was a Postdoctoral Research Fellow, first at the University of Florence and then at the University of Siena (Siena, Italy), from 2008 to 2010. From 2012 to 2021 he came back at the University of Florence as Assistant Professor, and there he currently is Associate Professor in Automation with the Department of Information Engineering. He serves as Associate/Academic Editor for scientific journals in the field of nonlinear systems, and he was in the committees of workshops and scientific congresses on the same subject. His main research interest is nonlinear dynamics with particular regard to networks of interacting agents and neuron models.

A. Tesi (M'76–SM'81–F'87) Alberto Tesi received the Laurea degree in Electronics Engineering from the University of Florence, in 1984, and the Ph.D. degree in Systems Engineering from the University of Bologna, in 1989. In 1990 he joined the Department of Systems and Computer Science of University of Florence, as a research assistant. He is currently a Professor of Control Systems at the Department of Information Engineering of University of Florence. He was associate editor of the IEEE TRANSACTIONS ON CIRCUITS AND SYSTEMS (1994-1995), IEEE TRANSACTIONS ON AUTOMATIC CONTROL (1995-1998) and Systems and Control Letters (1995-2010). He was member of the conference editorial board of the Conference on Decision and Control (1994-1999) and the American Control Conference (1995-2000), and member of the program committee of several international conferences. His research interests are in analysis of nonlinear dynamics of complex systems, robust control of linear systems and optimization. He is co-author of about 180 scientific publications.

M. Di Marco was born in Firenze, Italy, in 1970. He received the Laurea Degree in Electronic Engineering from the University of Firenze, Firenze, Italy and the Ph.D. degree from the University of Bologna, Bologna, Italy, in 1997 and 2001, respectively. From November 1999 to April 2000 he held a position as Visiting Researcher at LAAS, Toulouse, France. Since 2000, Dr. Di Marco has been with the University of Siena, Siena, Italy, where he is currently Associate Professor of Circuit Theory. He is author of more than 80 technical publications. His current research interests are in analysis and modeling of nonlinear dynamics of complex systems and neural networks, in robust estimation and filtering. From 2007 to 2011, Dr. Di Marco has been serving as Associate Editor of the IEEE TRANSACTIONS ON CIRCUITS AND SYSTEMS I: REGULAR PAPERS.

M. Forti received the Laurea degree in Electronics Engineering from the University of Florence, Italy, in 1988. From 1991 to 1998, he was an Assistant Professor in applied mathematics and network theory with the Electronic Engineering Department of the University of Florence. In 1998 he joined the Department of Information Engineering and Mathematics of the University of Siena, Italy, where he is currently Professor of electrical engineering. His main research interests are in the field of nonlinear circuits and systems, with emphasis on the qualitative analysis and stability of circuits modeling artificial neural networks. His research activity also includes aspects of electromagnetic compatibility. Dr. Forti served as Associate Editor of the IEEE TRANSACTIONS ON CIRCUITS AND SYSTEMS I: FUNDAMENTAL THEORY AND APPLICATIONS from 2001 to 2003 and of the IEEE TRANSACTIONS ON NEURAL NETWORKS from 2001 to 2010. He is currently serving as Associate Editor of the IEEE TRANSACTIONS ON CYBERNETICS, Neural Networks and Frontiers in Neuroscience.